Prediction of the Diurnal Cycle Using a Multimodel Superensemble. Part II: Clouds

ARINDAM CHAKRABORTY AND T. N. KRISHNAMURTI

Department of Meteorology, The Florida State University, Tallahassee, Florida

C. GNANASEELAN

Department of Meteorology, The Florida State University, Tallahassee, Florida, and Indian Institute of Tropical Meteorology, Pune, India

(Manuscript received 6 November 2006, in final form 19 March 2007)

ABSTRACT

This study addresses the issue of cloud parameterization in general circulation models utilizing a twofold approach. Four versions of the Florida State University (FSU) global spectral model (GSM) were used, including four different cloud parameterization schemes in order to construct ensemble forecasts of cloud covers. Next, a superensemble approach was used to combine these model forecasts based on their past performance. It was shown that it is possible to substantially reduce the 1–5-day forecast errors of phase and amplitude of the diurnal cycle of clouds from the use of a multimodel superensemble. Further, the statistical information generated in the construction of a superensemble was used to develop a unified cloud parameterization scheme for a single model. This new cloud scheme, when implemented in the FSU GSM, carried a higher forecast accuracy compared to those of the individual cloud schemes and their ensemble mean for the diurnal cycle of cloud cover up to day 5 of the forecasts. This results in a 5–10 W m^{-2} improvement in the root-mean-square error to the upward longwave and shortwave flux at the top of the atmosphere, especially over deep convective regions. It is shown that while the multimodel superensemble is still the best product in forecasting the diurnal cycle of clouds, a unified cloud parameterization scheme, implemented in a single model, also provides higher forecast accuracy compared to the individual cloud models. Moreover, since this unified scheme is an integral part of the model, the forecast accuracy of the single model improves in terms of radiative fluxes and thus has greater impacts on weather and climate time scales. This new cloud scheme will be tested in real-time simulations.

1. Introduction

Clouds contribute to a large modulation of the energy budget of the earth–atmosphere system. They change the energy balance through three-dimensional redistribution of radiation by taking part in the water cycle and indirectly contributing to latent heat release during precipitation. These effects together contribute to the surface and TOA (a list of acronyms is provided in Table 1) radiation budgets, surface temperature, heating rate in the atmosphere, and overall to the climate change.

Convection and cloudiness show large amplitude and coherent modes of variations at the diurnal time scale. The diurnal cycle can modulate the time-mean energy budget of the earth–atmosphere system. From radiative transfer calculations, Bergman and Salby (1997) showed that there can be large errors in the estimation of TOA shortwave flux (~20 W m^{-2}) and longwave flux (~5 W m^{-2}) if the diurnal variation of clouds was not taken into account. Moreover, diurnal variation of radiative fluxes drives the diurnal variation of surface wind and divergence (Dai and Deser 1999) and water cycle (Trenberth et al. 2003). Slingo et al. (2003) hypothesized that diurnal variation of sea surface temperature–induced convection can have an impact on the MJO. Bergman and Salby (1996), using ISCCP C2 datasets, showed that the diurnal cycle of clouds is dependent on the cloud climatology over that region. Thus, the diurnal and seasonal time scales interact with each other.

Diurnal cycles of convection and precipitation, in general, show the afternoon maximum over land and

Corresponding author address: Arindam Chakraborty, Department of Meteorology, The Florida State University, Tallahassee, FL 32306.
E-mail: arch@io.met.fsu.edu

DOI: 10.1175/2007MWR2080.1

TABLE 1. List of acronyms used in this paper.

CAPE	Convective available potential energy
CCSM2	Community Climate System Model version 2
CERES	Clouds and the Earth's Radiant Energy System
COADS	Comprehensive Ocean–Atmosphere Data Set
ECMWF	European Centre for Medium-Range Weather Forecasts
EFH	Eastern foothills of the Himalayas
ETP	Eastern Tibetan Plateau
FSU	The Florida State University
GCM	General circulation model
GSM	Global spectral model
IR	Infrared
ISCCP	International Satellite Cloud Climatology Project
MJO	Madden–Julian oscillation
MOS	Model output statistics
MRF	Medium-range weather forecast
NCAR	National Center for Atmospheric Research
NCEP	National Centers for Environmental Prediction
OLR	Outgoing longwave radiation
PBL	Planetary boundary layer
PFM	Protoflight Model
SST	Sea surface temperature
TOA	Top of the atmosphere
TRMM	Tropical Rainfall Measuring Mission

early morning maximum over ocean (e.g., Dai 2001). However, many studies depicted exceptions to this general tendency. For example, Shin et al. (1990) and Janowiak et al. (2005) showed that the convection maximum over oceans can occur during the afternoon hours. Wallace (1975) and Dai et al. (1999) found the nocturnal peak in precipitation over the central continental United States. This nocturnal peak was due to the eastward-propagating convective systems from the lee side of the Rocky Mountains (Betts and Jakob 2002b). A recent paper by Yang and Smith (2006) examined the characteristics of the diurnal cycle of precipitation from TRMM datasets. They found that the phase and amplitude of the diurnal mode of precipitation can vary with space and time both over land and ocean. Dai (2006) noted that there exists a small difference between the diurnal cycles of precipitation obtained from TRMM satellite–based estimates and that directly obtained from surface observations. Yang and Slingo (2001) pointed out that oceanic regions near the continents were influenced by the presence of land and the maximum of convection was found in the noon hours. Over land, the phase of the diurnal cycle can vary with surface type and orographic height. For example, over the eastern Tibetan Plateau, summer monsoon convection occurs in the afternoon hours, whereas a few hundred kilometers south of this region near the foothills of the eastern Himalayas, the convection maximum is in the early morning hours (Murakami 1983; Krishnamurti et al. 2007).

Variation of solar insolation is the driving force for the diurnal cycle. For example, diurnal variation of shortwave absorption at the cloud top can control the diurnal variability of the stability of convection (Bergman 1997). However, the actual mechanism behind the selection of phase and amplitude is rather complex. Over oceans, the observed diurnal cycle of precipitation can be qualitatively accounted for by direct radiative–convective interactions (Randall et al. 1991). Moreover, indirect radiative–convective interactions mediated by large-scale dynamics and the remote influence of land also play roles in the diurnal phase selection. Randall et al. (1991) showed that diurnal cycle of large-scale vertical motion is an effect rather than a cause behind the diurnal variation of precipitation. Dai et al. (1999) showed that over the continental United States, near the Rocky Mountains in the west and over the southeast region (over Florida), there exists a strong afternoon maximum in the diurnal cycle of summer precipitation. This is due to static instability and surface convergence resulting from diurnal variation solar heating. Over the central Great Plains of the United States, low-level large-scale convergence suppresses daytime convection and favors nighttime convection. The nocturnal convective intensity over this region is enhanced by eastward-moving thunderstorms (Dai et al. 1999). Using 3-hourly weather reports from around the globe and COADS during 1975–97, Dai (2001) showed that the afternoon maximum of showery precipitation over land results from high CAPE due to daytime solar heating. The early morning maximum of nonshowery drizzle over land was found to be associated with high relative humidity and low temperature at those hours of the day. Dai (2001) suggested that the early morning maximum in precipitation over oceans adjacent to continents is induced by diurnal variation over land areas (with an opposite phase), whereas the diurnal cycle over ocean far away from lands is influenced by pressure tide as well as variation in relative humidity. Further understanding of the albedo of high clouds is also needed since that can play a role in stabilizing the upper part of vertical columns. However, a simple theory may not explain many characteristics of the diurnal cycle that are observed over land and the oceans, which may depend on surface–radiation–cloud interactions and the life cycle of clouds themselves (Chen and Houze 1997).

Because of the well-defined coherent geographical and temporal variations and the complexity of the mechanisms, the prediction of the diurnal cycle is a good test bed for different physical processes in a GCM (Yang and Slingo 2001; Dai and Trenberth 2004). Current GCMs have considerable difficulties in forecasting

the diurnal cycle of cloud cover (e.g., Randall et al. 1991; Yang and Slingo 2001; Dai and Trenberth 2004) and radiative fluxes (e.g., Slingo 1987; Betts and Jakob 2002a). One of the obvious reasons is in the deficiencies of cloudiness parameterization. Dai and Trenberth (2004) examined the performance of the NCAR CCSM2 cloud scheme in simulating the diurnal cycle. One of the objectives of the present study is to compare performances of several different cloud parameterization schemes in forecasting the diurnal cycle of cloud cover.

The main purpose of this study is to develop a new cloud parameterization scheme for global climate models and to test its performance for forecasting and simulating the diurnal cycle of clouds and radiative fluxes at the TOA. The forecasting of the diurnal cycle of clouds is also being addressed here using a multimodel superensemble (SE) technique (Krishnamurti et al. 1999). Previous studies have shown that the superensemble can provide somewhat higher accuracy for hurricane forecasts (Krishnamurti et al. 1999; Williford et al. 2003), numerical weather prediction (Krishnamurti et al. 2003; 2000), and seasonal climate forecasts (Yun et al. 2003; Krishnamurti et al. 2006a,b; Chakraborty and Krishnamurti 2006) compared to the members of a suite of models. All the accuracy measures were estimated using the ISCCP datasets for clouds and the CERES datasets for radiative fluxes as the benchmarks.

In the next section, a brief overview of the ISCCP datasets is presented. Section 3 outlines the experimental details. The new unified cloud parameterization scheme is described in section 4. Section 5 demonstrates the workings of the superensemble methodology (i.e., a step-by-step illustration of the forecast steps at a single point). Forecast accuracies of the member models utilizing individual cloud schemes, the multimodel superensemble, and the unified scheme for predicting the diurnal cycle of low and high clouds are presented and compared in section 6. Forecasts of monthly mean radiative fluxes are presented in section 7. The main results of the study are summarized in section 8 with a note toward future possibilities.

2. ISCCP datasets

This study used ISCCP DX1 pixel datasets (Rossow and Schiffer 1999) for forecast validation purposes. There were 5 geostationary satellites and 16 polar orbiting satellites available during our study period (January–March 2000). These satellites together covered all parts of the globe. These DX1 pixels carried a 30-km spatial resolution and were available at intervals of every 3 h. Among other variables, ISCCP DX1 datasets provided a binary flag that declared a pixel to be either cloudy or clear. These cloud detection results were available separately for the visible and IR wavelengths. The visible threshold results were available only at daytime hours, whereas the IR threshold results were available both during day and night hours. Rossow et al. (1993) and Rozendaal et al. (1995) showed that there can be considerable differences in the cloud fractions using only the IR thresholds versus those from the visible adjusted IR (VIS/IR) thresholds. We have used only the IR threshold results to estimate the cloud fractions because one of the main purposes of this study is to forecast the diurnal variation of cloud cover, which requires data of similar characteristics both during day and night. We expect that bias in the IR data that possibly arises from algorithm or instrumental problems (a possible constant bias during day and night) would cancel out when we use IR both during the day- and the nighttimes, since the mean was removed prior to the calculation of the diurnal cycle. However, over land there can be significant error in the ability of the IR thresholds to identify especially low clouds, as pointed out by Bergman and Salby (1996). This kind of error in the IR detection of low clouds over land cannot be corrected using the method adopted in this study.

If data from more than one satellite are available over a grid at a certain hour of the day, the data to be used were determined from a hierarchy of preferences of the satellites. Geostationary satellites get preference in the region of 55°S–55°N. This processing technique was very similar to that used to produce the ISCCP equal area (280 km) cloud fractions from DX1 pixels (described in the ISCCP cloud dataset user's guide).

Cloud fractions at a transformed model grid (~0.94° in the FSU GSM; Krishnamurti et al. 2007) were defined as the total number of cloudy pixels divided by the total number of nonoverlapping pixels within that grid location. Different cloud types were detected from the cloud-top pressure of the cloudy pixel. Low clouds can exist below 700 hPa, middle clouds can exist between 700 and 400 hPa, and high clouds can exist above 400 hPa. We define the cloud fraction of a certain cloud type (low, middle, or high) as the total area covered by cloudy pixels having cloud-top pressure within the range of that cloud type divided by the total area of that grid. No overlapping assumption was made to calculate low-, middle-, and high-cloud fractions from ISCCP satellites. It was noted (e.g., Dai et al. 2006) that there exist problems in cloud fractions estimated from ISCCP satellites. Since ISCCP satellites were unable to sense radiance from the layers below in the case of the existence of high clouds, the fraction of low and middle

TABLE 2. Main features of the four diagnostic cloud parameterization schemes used in this study.

Name	Origin	Main features
FSUold	FSU global spectral model	(i) Relative humidity threshold
FSUnew	FSU global spectral model	(i) Relative humidity threshold (ii) Correction of convective cloud amount from precipitation
NCAR	NCAR CCM3	(i) Relative humidity threshold (ii) Correction of convective cloud amount from precipitation (iii) Special treatment of layered clouds
PX	Pleim and Xiu (1995) scheme from the fifth-generation Pennsylvania State University–NCAR Mesoscale Model (MM5)	(i) Relative humidity threshold (ii) Threshold is a function of height for each cloudy type

clouds could have been underestimated in such situations. This was a potential source of errors in the ISCCP dataset that was used in this study. However, we expect that this error was not large enough to change the diurnal characteristics of the ISCCP estimated cloud fractions used in this study. Moreover, given a more accurate dataset from ISCCP satellites during the training period, the superensemble and the unified cloud scheme can perform better compared to their performances presented in this paper (Krishnamurti et al. 2003). The final outcome of this data processing provided global equal-angle gridded 3-hourly cloud fractions from ISCCP satellite–based estimates.

3. Experimental details

This study used four available cloud parameterization schemes. Table 2 gives an overview of these schemes. All these schemes calculated cloud fraction diagnostically from large-scale parameters such as relative humidity. These cloud schemes varied in the exact definition of different cloud types in the model. For example, FSUold did not correct convective cloud amount from the precipitation rate, which was a feature of the FSUnew and NCAR cloud schemes. Krishnamurti et al. (2007) described all these cloud schemes in further detail. These variations in the exact details enabled this ensemble of cloud schemes to provide a robust spread in the amount of cloud fraction and independent sampling for the construction of the superensemble. It was our original intension to include a prognostic cloud scheme as well that includes and predicts (as dependent variables) cloud fractions and the liquid water mixing ratio (e.g., Sundqvist 1978; Sundqvist et al. 1989). However, upon the construction of the ensemble and unified scheme we noted that much improvement can come for the modeling and forecasting of the diurnal change from the use of these simple diagnostic cloud schemes. Hence, this study was limited to the use of a suite of diagnostic cloud schemes.

The FSU GSM was used here to construct ensemble forecasts with four different cloud schemes. The model used triangular truncation at 126 waves (T126), which corresponds to roughly 0.94° grid separation in the physical space. It had 27 vertical sigma levels with more closely spaced levels near the surface and at the tropopause. The main features of the model are given in Krishnamurti et al. (2007). To construct ensemble forecasts, all other components of the model except the cloud parameterization scheme were kept unchanged between different members. Five-day-long forecasts were made with all four versions of the model starting at 1200 UTC 1 January 2000–31 March 2000. Initial conditions were extracted from the 40-yr ECMWF Re-Analysis (ERA-40). SSTs were obtained from Reynolds and Smith's (1994) weekly datasets and interpolated to the model run time.

Outputs of the model were stored at 3-hourly intervals (at 0000, 0300, . . . , 2100 UTC) for estimating the diurnal cycle. Starting at 1500 UTC of the day of the model start until 1200 UTC of the next day, all of these eight (3 hourly) forecast time points together were designated as day-1 forecasts in this study. Day-2 through day-5 forecasts follow similarly. A time series of the day-n ($n = 1, 2, \ldots, 5$) forecasts was created by joining the string of day-n forecasts from 91 separate forecasts for each member of the ensemble.

To construct the superensemble forecasts for day n, the time series of the day-n forecasts was divided into a training period and a forecast period. The details of the superensemble methodology are given in Krishnamurti et al. (2007). The training period was limited to the first 81 days. The last 10 days constituted the forecast phase. Eight sets of separate statistical weights were calculated for every 3 h of the day by regressing the forecasts valid at that hour against corresponding ISCCP-based satellite estimates. This provided 40 different sets of weights, one for every lead time and every 3 h of the day from day-1 to day-5 forecasts. Different weights at different lead times for different hours of the day ac-

count for any systematic change in bias of the member cloud schemes. Finally, superensemble forecasts for day n were constructed using the eight weights thus obtained and valid for day n. These weights vary geographically and were calculated at every grid location of the models.

A Fourier transform on the time series of 3-hourly forecasts was made on every day of the series to extract the diurnal cycle. The diurnal cycle is defined here as the first harmonic of the transformed series. Next, hour-by-hour averages of the first harmonic of the filtered data over the total number of forecast days were calculated in order to construct the diurnal cycle of the entire forecast time series. It was found that the diurnal cycle obtained using this method was in fact very close to the nth harmonic of an n-day-long string of time series of data. Here n refers to 1 through 5.

4. Design of a unified cloud parameterization scheme

This study developed a new cloud parameterization scheme that used the idea of superensembles. The superensemble technique (Krishnamurti et al. 1999, 2000) constructs a consensus forecast from a set of multimodel forecasts. The consensus forecast is made by combining the available member models with different weights. Weights are determined from past performances of the models. The constructed superensemble forecast is

$$S = \overline{O} + \sum_{i=1}^{N} a_i(F_i - \overline{F}_i), \tag{1}$$

where $\overline{O}$ is the observed climatology, a_i is the weight for the ith member in the ensemble, and F_i, $\overline{F}_i$ are the forecasts and forecast climatological values for the ith model's forecast, respectively. The summation is taken over the N member models of the ensemble. Superensemble methodology is described in detail in Part I of this paper (Krishnamurti et al. 2007). It is an MOS-based forecast technique that maps the model attractors to the atmospheric attractor. There are other MOS-based ensemble forecast methodologies that correct the bias of the member models depending on their past performance to provide a bias-removed forecast. Yussouf and Stensrud (2006) used 12 days of observations and model forecasts to estimate the bias of each model of their study. These biases were then used to correct the persistent errors in forecasting the near-surface variables from the models. Hamill et al. (2004) used a version of the MRF model from NCEP to issue retrospective probabilistic forecasts. Statistical correction of the model errors produced large improvements in the forecast skills. The superensemble methodology is different compared to other MOS-based forecasts in that here differential weights are assigned to the member models based on their past performance. This idea of differential weights enables the superensemble to assign higher weight to a "good" model as compared to a "bad" model. It was found that this procedure outperforms the bias-removed ensemble mean (EM) forecasts (Stefanova and Krishnamurti 2002; Chakraborty and Krishnamurti 2006) both in terms of probabilistic and deterministic performance measures.

It was possible to use the notion of the superensemble to construct a new cloud parameterization scheme that was a consensus of all the member parameterization models. This idea of a unified scheme was first developed by Krishnamurti and Sanjay (2003) from a collection of member cumulus convection parameterization schemes that provided better representation of convection compared to the individual convection schemes in forecasting precipitation and the vertical profiles of heating and drying.

Figure 1 schematically outlines the steps of forecasting of clouds with a single parameterization scheme, with the superensemble, and with the unified scheme. In a single model forecast, one cloud parameterization scheme was used within that model. This provided an ensemble of four member models with different cloud forecasts (Fig. 1a).

To construct a superensemble, all the single model forecasts for low, middle, and high clouds were separately collected and their weights were calculated based on their past performances. These weights varied geographically. They were then used to combine all four sets of member model forecasts. This way, a single consensus superensemble forecast was obtained for each of the cloud types (Fig. 1b).

The unified scheme was built within a single model where the weighted sum of the cloud schemes was used (Fig. 1c). This exercise was started with a calculation of weights of the member models for three different cloud types (low, middle, and high) for the months of January and February 2000. This method for the calculation of weights was identical to that used for the construction of the superensemble, except that the training period for the superensemble was from 1 January to 21 March. This change in the length of the training period did not have any significant influence on the weights of the models since superensemble weights stabilize when the length of the training period exceeds about 45 (Krishnamurti et al. 2003). In the present case, the training length for the superensemble was 81 and that for the unified cloud scheme was 60. ISCCP cloud fractions

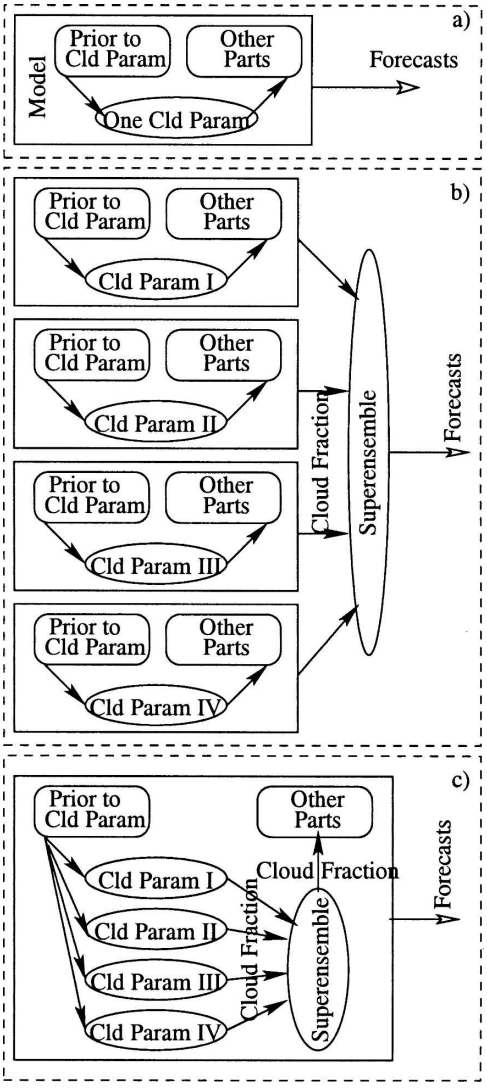

FIG. 1. Schematic representation of the methodology of forecasts with (a) a single cloud parameterization scheme, (b) the superensemble scheme, and (c) the unified cloud parameterization scheme.

were extracted for validation purposes. A single set of weights was obtained for each of the 3 h of forecasts during a day and at each forecast lead time. In the next step, all four schemes were run in parallel as an integral part of one model to obtain the predicted cloud fractions (Fig. 1c). Outputs from these cloud parameterization schemes included the cloud fractions for each layer of the model. These weights for different cloud fractions, calculated previously, were applied to a single model to construct a unified forecast. All the layers below the 700-hPa level utilized the weights calculated for the low cloud fraction. Layers between 400 and 700 hPa utilized weights for middle clouds and layers above 400 hPa utilized weights for high clouds. Unified cloud fractions were calculated for each of these layers of the model. These cloud fractions were then passed on to the other parts of the model (e.g., shortwave and longwave radiation calculations) and interacted fully as the forecast evolves. The unified cloud scheme increased the computing time of the model runs only minimally. Here it should be noted that since cloud parameterization routines are relatively simple compared to other parameterization routines like the PBL, the increase in computational time may be relatively higher when a unified parameterization model is created with a number of PBL schemes. However, since a parameterization routine is only one of the several parts of a global model, a small-to-moderate increase in computational time while running a unified model will have a negligible effect on the overall computational time of the model. Another concern with reference to a unified scheme is the reduction of the variance of cloud fraction due to averaging. The present study focuses on a particular mode of time variation of cloud fraction (viz., the diurnal mode) and therefore does not have a chance to discuss the change in the variance in cloud fraction in detail. However, it was noticed that over the Australian monsoon region (20°S–0°, 120°–140°E) during the end of March 2000, the variance of high clouds from the unified scheme was within the spread of the variances from the individual member models (variances from four member models and the unified cloud scheme were 0.8%, 0.5%, 3.2%, 6.0%, and 0.6%, respectively). Therefore, there was no large reduction in the variance because of the construction of the unified cloud scheme from a weighted average of the member model cloud fractions.

This new cloud parameterization scheme was statistical–physical based. It combined the physically based parameterization schemes based on their local past performances. This cloud scheme was designed to correct the best parameterization scheme of the suite of models. Since this scheme was flexible in terms of the number of models in the ensemble, any number of input member models can, in principle, be used to construct the unified scheme. Krishnamurti et al. (2003) and Chakraborty and Krishnamurti (2006) showed that the performance of the superensemble increased if better models were used for the input. Thus, a better set of cloud parameterization schemes in the input suite of member models can enhance the forecast accuracy of the unified cloud parameterization scheme. This new unified scheme was an integral part of one model and thus had the potential to improve forecasts of other parameters of the model, in addition to the variable upon which the scheme was built.

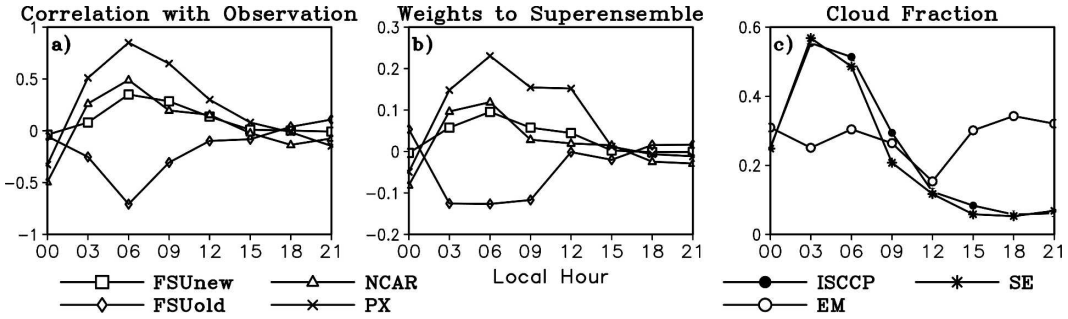

FIG. 2. Illustration of the performance of member models over a grid point (18°S, 133°E) for low cloud and the need to assign different weights to the member models based on their performance: (a) cross correlation of the model-simulated low cloud fraction with that of the ISCCP at each hour during the training period, (b) weights assigned to the member models at each hour to construct the SE, and (c) ISCCP satellite–based estimates of low cloud and predicted low cloud by the ensemble mean of the models and the SE. Legends are same for (a) and (b) and separate for (c).

5. A walk through a superensemble forecast

In this section we illustrate the workings of the superensemble. Figure 2 shows an example of such forecasts over a single grid point located at 133°E and 18°S (over sea). The time line was divided into two parts: the first 80 days for the training period and the next 10 days for the forecast period. Figure 2a shows the correlations during the training period between the model-predicted low cloud anomaly and the ISCCP counterpart. This parameter can be considered as a yardstick for the performance of the models. At hours 1500–2100 LT (local sun time), all the models had very low correlations. From 0300 to 1200 LT, FSUold showed negative correlations whereas the other three models showed positive correlations.

Figure 2b shows the weights that were assigned to these models at each 3-hourly interval for the construction of the superensemble. Note that all the models had nearly zero weights from hours 1500 to 0000 LT, which was consistent with the "no correlation" with ISCCP datasets during this time (Fig. 2a). From 0300 to 1200 LT, FSUnew, NCAR, and PX carried positive weights since they had positive correlation with ISCCP datasets. Moreover, PX carried higher weights compared to FSUnew and NCAR because the former had higher correlation compared to the other two models. On the other hand, during 0300–0000 LT, NCAR carried negative weights. Note from Fig. 2a that this model showed negative correlation with the ISCCP datasets during this period. Therefore, according to Eq. (1), its anomaly should be multiplied by a negative number to correct the forecast anomalies. The final superensemble forecast is the sum of all the anomaly forecasts multiplied by their respective weights plus the long-term mean observed estimates during the training phase.

Such consensus forecasts, when compared with the simple equal weight ensemble mean, provided enhanced performances. Figure 2c shows the average superensemble forecasts for these set of weights. Note that the ensemble mean hardly showed any variations in low cloud amount during a day. Superensemble-predicted low-cloud fractions were very close to the ISCCP estimates for all hours. This included the peak at early morning and no-cloud conditions in the afternoon hours. This kind of improvement in the consensus ensemble forecasts had been possible because of the assignment of differential weights to the member models based on their performance during the training period.

6. Results

a. Phase and amplitude over the Tropics and subtropics

Figures 3 and 4 show the absolute phase errors of the diurnal cycle of low clouds from the member cloud models, their ensemble mean, the unified cloud scheme, and the superensemble during 22–31 March 2000 for days 3 and 5 of the forecasts, respectively. The numbers above each panel indicate the domain mean absolute errors in phase. All four member cloud schemes and their ensemble mean showed large errors both over land and the oceans except for a few regions like the north-central Pacific Ocean near 120°W and 15°N. Errors during day 5 were relatively higher as compared to day 3 in general. The unified scheme and superensemble showed very low phase errors both over land and the oceans as compared to the member cloud schemes. The mean phase error for the unified cloud scheme was 2.6 and 2.5 h for day 3 and day 5 of the forecasts, respectively. The phase error reduced further for the superensemble (1.9 and 1.8 h, respectively, dur-

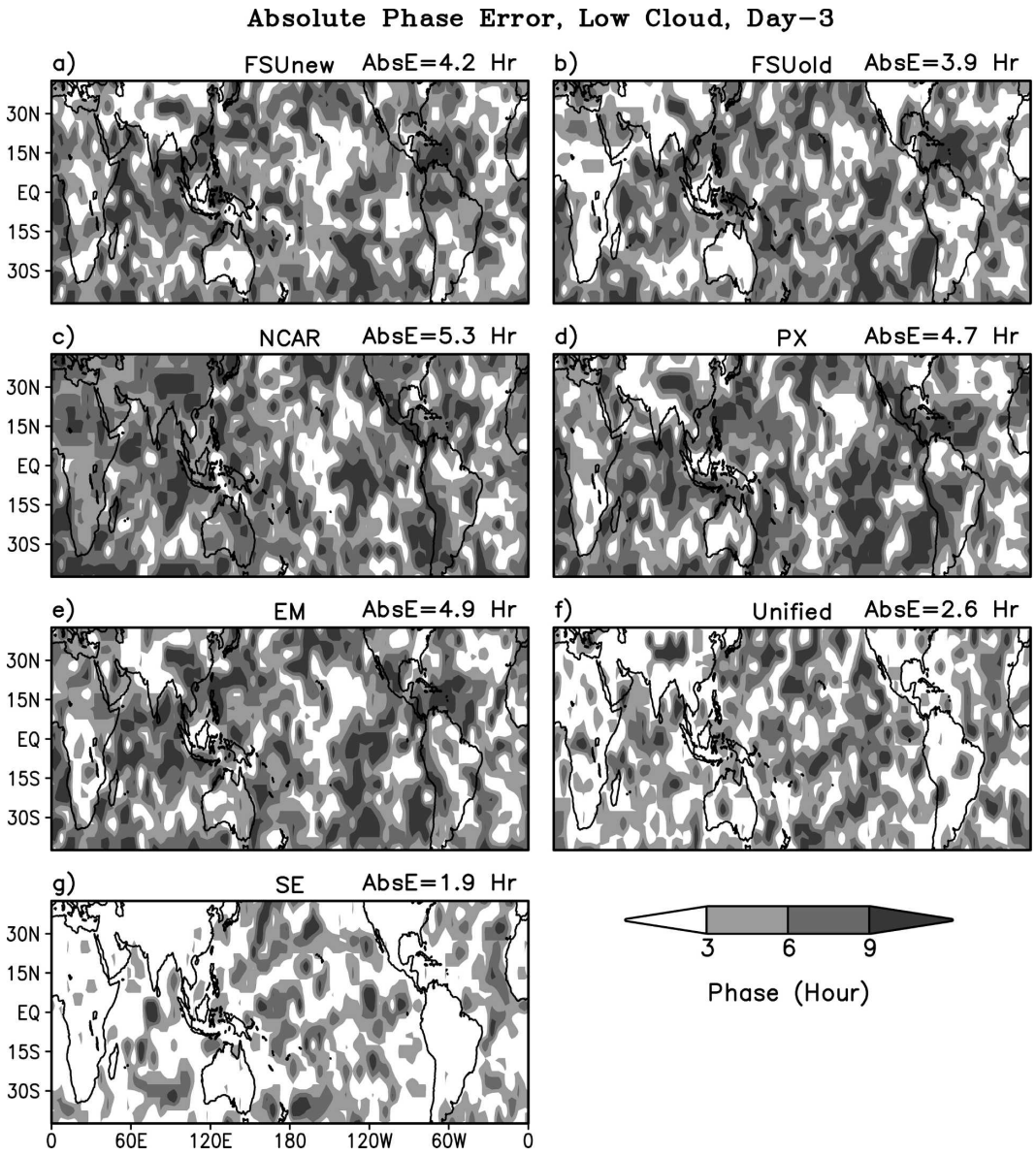

FIG. 3. Absolute phase error of low clouds for day 3 of forecasts from the member models, EM, unified scheme (Unified), and SE during 22–31 Mar 2000. Area mean absolute error in phase is indicated at the top of each panel.

ing days 3 and 5 of forecasts). This slight reduction in domain mean phase errors both for the unified scheme and the superensemble during day 5 as compared to day 3 was probably due to a more consistent bias in the member models during day 5.

Errors in the amplitude of the diurnal cycle of low clouds (Figs. 5, 6) showed a very clear land–ocean contrast, the higher errors being over land as compared to those of the oceans. Only the NCAR cloud scheme showed relatively low errors both over land and the oceans. The FSUnew, FSUold, and PX cloud schemes underestimated the amplitude over land by as much as 3.6% and overestimated the amplitude over ocean far from land (mid–Pacific Ocean) by 1.2%. The ensemble mean of the cloud schemes showed similar error structures to those of the individual schemes (rms error of amplitude = 4.7%). The unified scheme performed somewhat better than the individual models (rms errors are 4.0% and 3.9% during days 3 and 5, respectively). Superensemble forecasts were clearly superior to all of the member models, their ensemble mean, and the unified scheme in terms of amplitude of the diurnal cycle (with rms error as low as 2.5%).

Figure 7 statistically measures the difference in am-

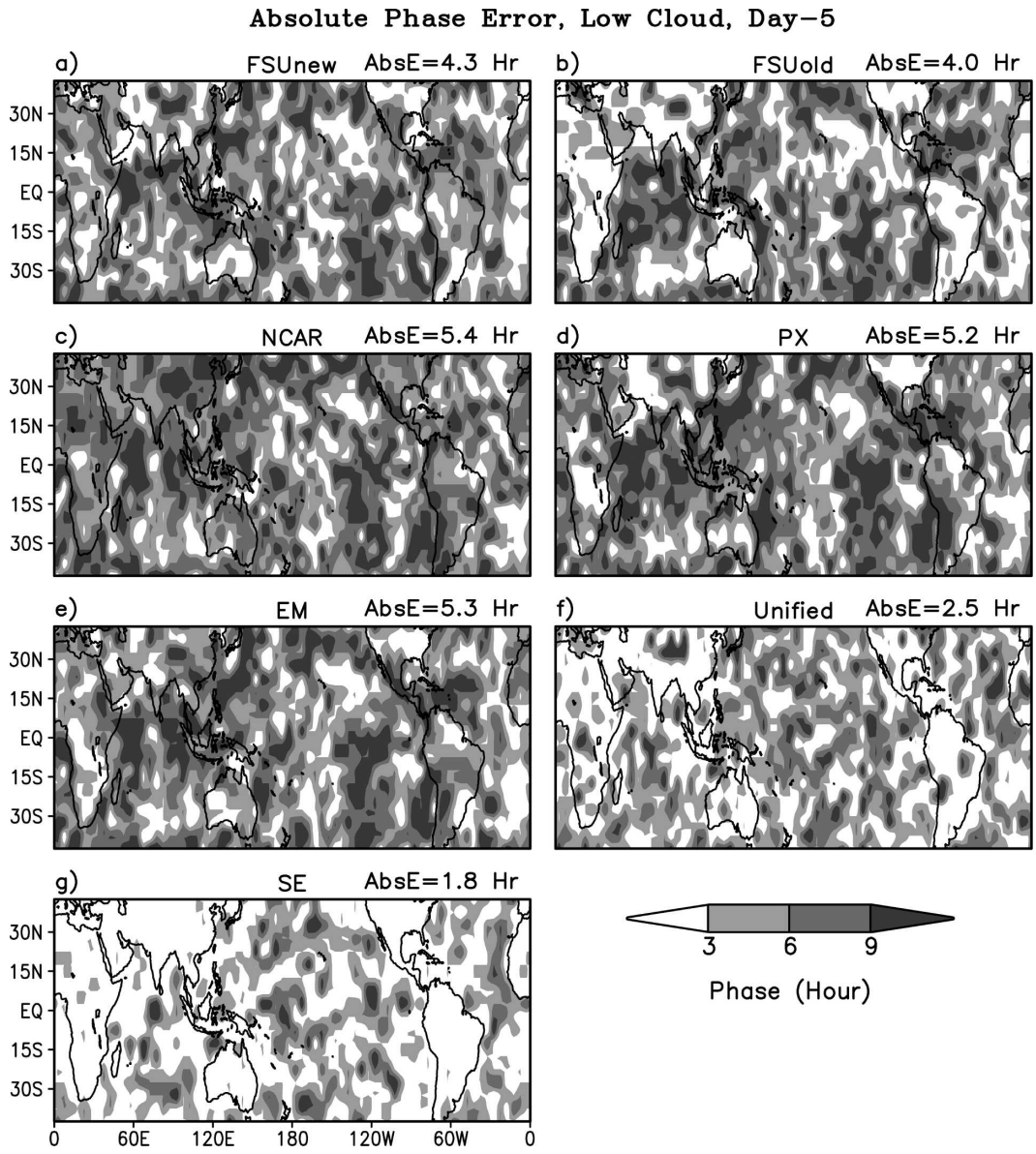

FIG. 4. Same as in Fig. 3 but for day 5.

plitude forecasts during days 3 and 5 from the superensemble and the ensemble mean. In this figure the shaded regions show where the superensemble amplitude was closer to that obtained from ISCCP satellite–based estimates and is different from the amplitude of the ensemble mean forecasts at a confidence level of 95%. This was computed using a *t* test (Chakraborty and Krishnamurti 2006). Over most of South America, East Asia, eastern North America, and South Africa, the amplitudes of the diurnal cycle of low clouds from the superensemble were better than those of the ensemble mean at the 95% confidence level. Similar features were found over different ocean basins. Notice that while going from day 3 to day 5 of forecasts (Figs. 7a,b), the superensemble retained its higher performance over the ensemble mean for the amplitude forecasts of the diurnal cycle of low clouds.

b. Diurnal cycle over the entire Tropics

A summary of the diurnal cycle of high clouds over all tropical (30°S–30°N, 0°–360°) land and ocean is shown in Fig. 8. Over land, the ISCCP satellite estimations showed a peak in the evening (2100 LT) with amplitude close to 4%. The NCAR and PX cloud schemes were able to forecast this phase somewhat realistically but the predicted amplitudes were off by a

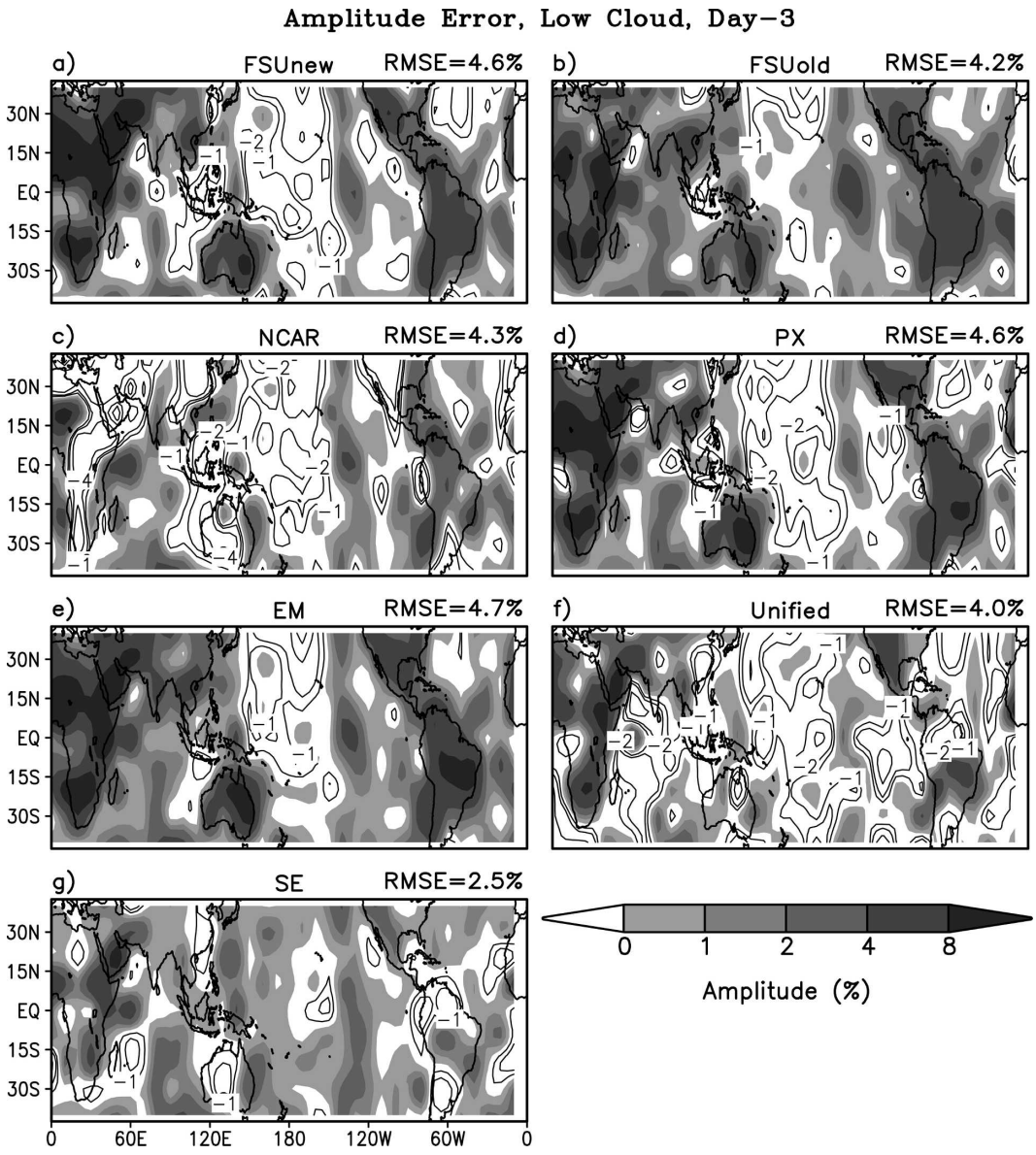

FIG. 5. Error in amplitude of low clouds for day 3 of forecasts from the member models, EM, Unified, and SE during 22–31 Mar 2000. RMS error over the entire domain is indicated at the top of each panel.

factor of 2–3. The ensemble mean, which carried a peak at 2100 LT, also underestimated the amplitude by a large margin. The RMS errors of the total diurnal cycle from the ensemble mean were 2.0% and 2.5% during days 3 and 5, respectively. The unified cloud scheme and the superensemble showed very high accuracy in predicting the diurnal cycle of high clouds over land. Both these forecasts carried phase and amplitudes close to the ISCCP estimates (RMS errors of the total diurnal cycle were around 0.1%).

Over oceans (Figs. 8b,d), high clouds showed a peak at 1500–1800 LT in the ISCCP-based satellite estimates. None of the member models were able to forecast this phase correctly either during day 3 or during day 5 of forecasts. As a result, the ensemble mean also had very large errors (rms error = 1.0%). The diurnal cycles from the unified scheme and the superensemble were very close to that of the ISCCP with phase at 1500 LT and amplitude close to 1% during day 3 as well as during day 5 of forecasts (rms errors = 0.1% and 0.2%, respectively). It was noted that this afternoon maximum of the high clouds occurred a few hours later than the precipitation maximum (Krishnamurti et al. 2007). This was consistent with the observation by Tian et al.

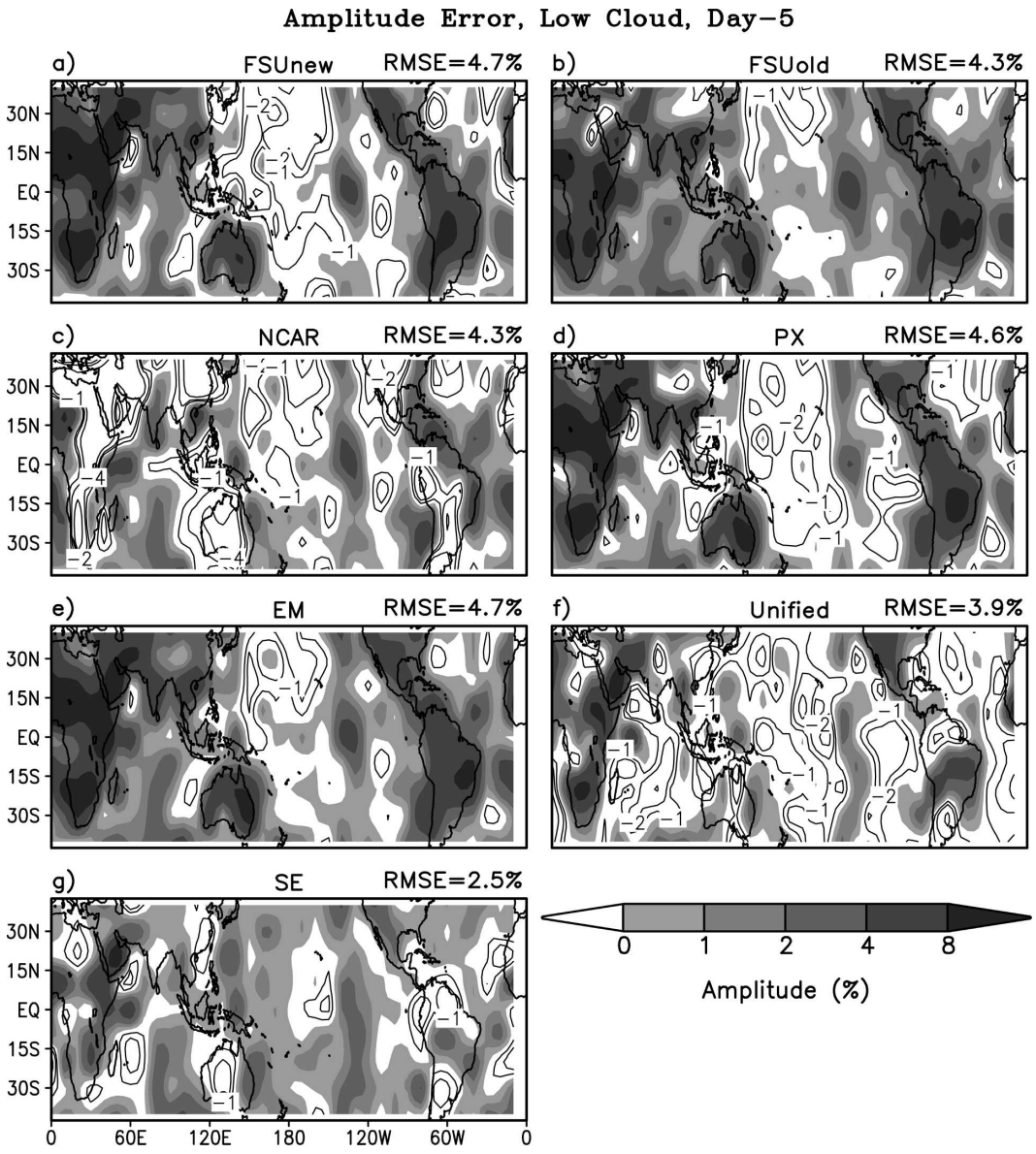

FIG. 6. Same as in Fig. 5 but for day 5.

(2004) that the phase of high clouds (which was during afternoon over ocean) followed the phase of convective precipitation by a few hours. This result shows that the unified cloud scheme, formulated in this study, and the superensemble both had a coherent mode of diurnal variation of high clouds similar to the observations up to at least 5 days in advance.

c. *Zonal propagation of cloud cover following the sun along the equator*

The diurnal cycle of low and high clouds has a strong land–ocean contrast both for phase and amplitude. This is due to different response times to the solar heating and different physical mechanisms that are responsible for the diurnal cycle over land and ocean. It is of interest to ask how the intensity of clouds follows the sun during a day longitudinally and how this intensity changes as the overhead sun moves from ocean to land and vice versa. This follows a representation of data proposed by Janowiak et al. (2005).

Figure 9 shows one such example for day 5 of forecasts along the equator (averaged between 10°S and 10°N) during 22–31 March 2000. In this figure, the horizontal axis represents the longitude and the vertical axis shows the local hours. No frequency filtering was performed to illustrate these results. At first a mean daily

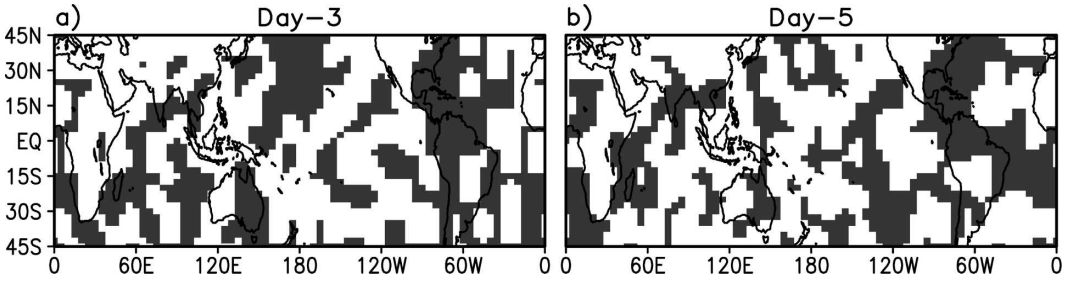

FIG. 7. Shaded regions show where the amplitude of low cloud from SE was superior to that of the EM by more than the 95% confidence level using a *t* test for days 3 and 5 of forecasts during 22–31 Mar 2000.

variation of high clouds over each grid box was computed for this 10-day period. Next the total cloud fraction of this mean daily variation was used to calculate the percent of occurrence of high clouds at intervals of every 3 h. Now, the average of this percent of occurrence over 10°S–10°N was plotted to show the relative occurrence of high clouds during different hours of a day. The shading in this figure starts for values above 12.5%. Note that this would have been the value at each 3-h interval if the high could cover were equally distributed (constant) over a day. Also shown is the fraction of land area between 10°S and 10°N as a function of longitude at the bottom panel. This figure shows that the phase of the diurnal cycle of high clouds can be different over different land areas (Fig. 9a). For example, over the equatorial African land (10°–40°E), the peak was at 1800–2400 LT, whereas over the central American landmass (280°–320°E) the peak occurred between 1500 and 2100 LT. In the ensemble mean data of the four cloud schemes (Fig. 9b), the peak of high

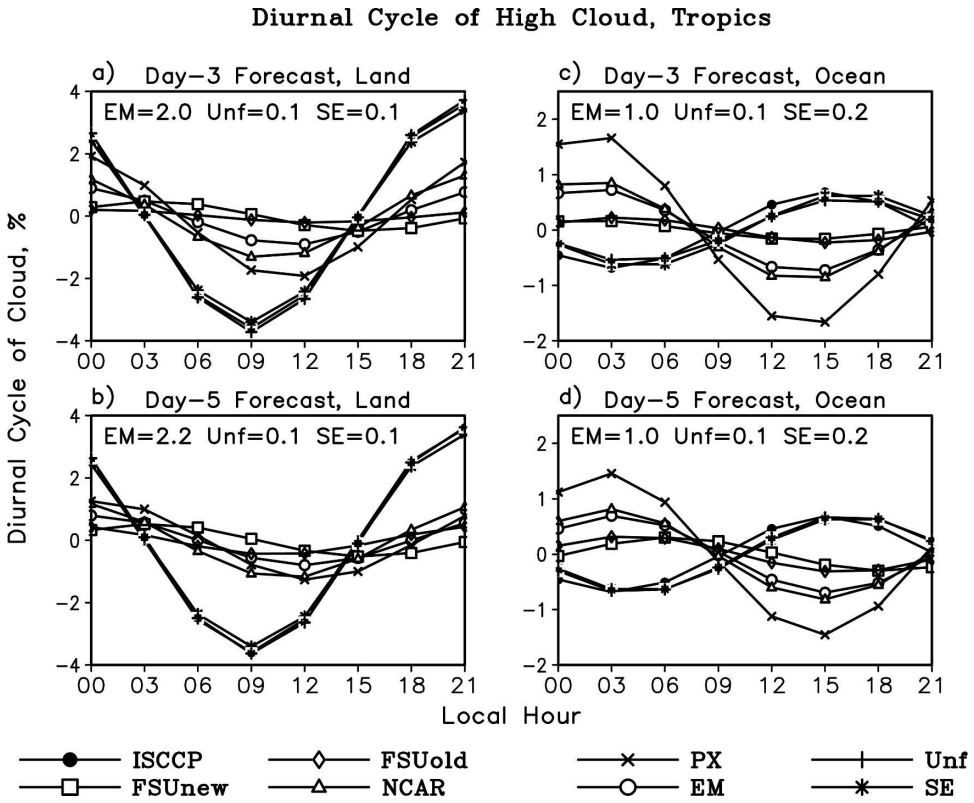

FIG. 8. Diurnal cycle of high cloud cover over the Tropics (30°S–30°N, 0°–360°E) from ISCCP and day 3 and 5 of forecasts from the member models, EM, Unified, and SE during 22–31 Mar 2000. The rms errors (%) of the total diurnal cycle for EM, Unified, and SE are indicated at the top of each panel.

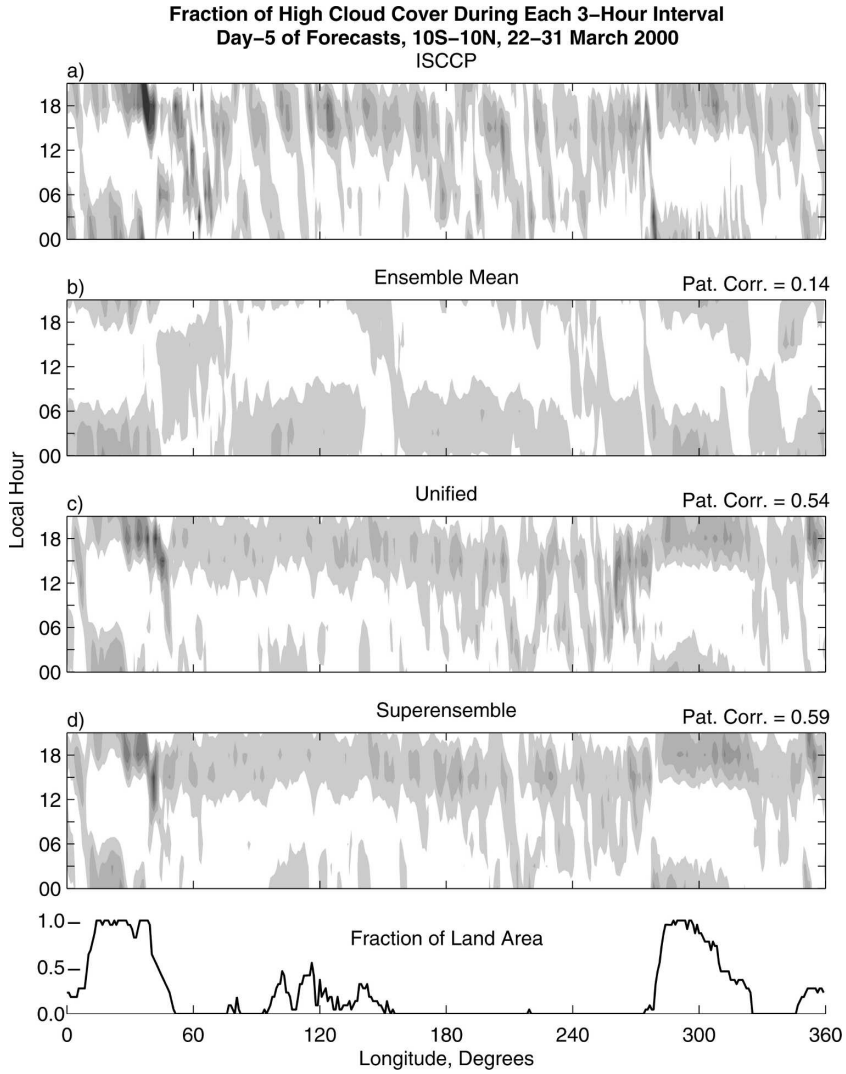

FIG. 9. Percent of high cloud cover during 8 octets (3-h intervals) of a day averaged between 10°S and 10°N from ISCCP and day-5 forecasts of EM, Unified, and SE during 22–31 Mar 2000. Pattern correlation of the forecasts against the ISCCP is shown at the top of each panel. (bottom) The fraction of land over that latitude belt. The vertical axis is in local solar time. The shading starts at 12.5%, which would have been the percent of cloudiness at each 3-h interval if cloud fractions were constant throughout the day (darker shade represents higher cloud amount).

cloud cover over equatorial Africa was delayed by 6 h (peak at 0000–0300 LT). Moreover the intensity of the peak was not as strong as it was in the ISCCP data. This suggests that for the ensemble mean the high cloud cover was somewhat equally distributed covering all hours of the day. The unified cloud scheme and the superensemble (Figs. 9c,d) both were close to the observation in predicting these peak hours and intensity of high clouds over the equatorial African and American continents.

Over the oceans, observed high cloud cover was nearly uniformly distributed all through the day, suggesting a weak diurnal cycle as was seen in Fig. 8. Moreover, the occurrence of the peak of this weak cycle varied from one basin to the other. Over equatorial Pacific Ocean (150°–270°E) the peak occurred at around 1500 LT (Fig. 9a). On the other hand, over the equatorial Indian Ocean (50°–90°E), the peak was at around 0600 LT. It was also noticed by Krishnamurti et al. (2007) that precipitation over the Indian Ocean occurred earlier than that over the Pacific Ocean. The day-5 ensemble mean forecast (Fig. 9b) showed a very weak hourly variation of high cloud cover. The unified scheme was able to forecast this land–ocean contrast of

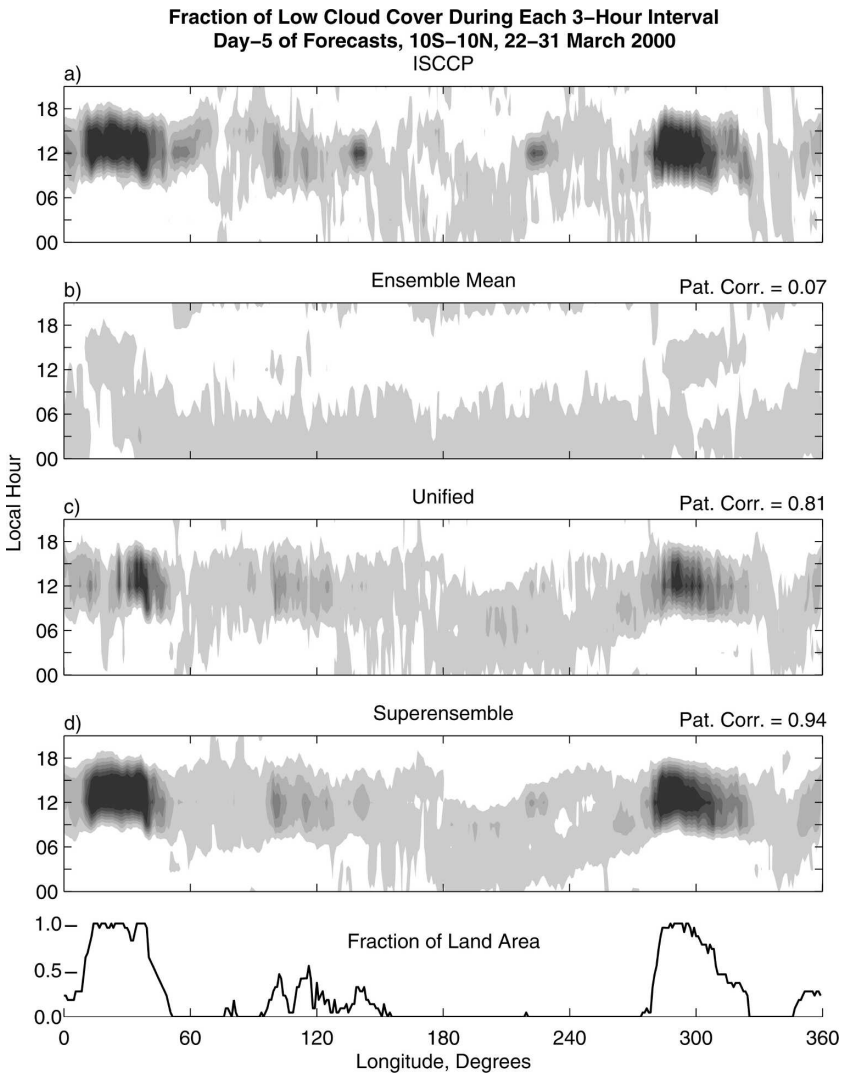

FIG. 10. Same as in Fig. 9 but for low cloud cover.

high cloud near the equator reasonably well (Fig. 9c). Superensemble forecasts over different ocean basins (Fig. 9d) were also very close to the observed estimates by the ISCCP satellites. Overall, the pattern correlation with ISCCP of this diurnal change of high cloud for the day-5 forecast was 0.14 for ensemble mean, 0.54 for the unified scheme, and 0.59 for the superensemble (these parameters are indicated above the respective panels).

Low clouds showed a different phase and amplitude of the diurnal cycle over the same latitude range (Fig. 10). Over land, the peak was found at 1200 LT as opposed to 2100 LT for high clouds. But similar to the high clouds, the amplitude over land was higher compared to that of the oceans. The ensemble mean of the four cloud schemes poorly represented the pattern of diurnal variation of low clouds (Fig. 10b). Ensemble mean forecasts showed the same magnitude of diurnal variation over land and the oceans. The overall pattern correlation of the ensemble mean forecast with the ISCCP was 0.07. The unified cloud scheme and the superensemble showed much higher accuracy toward predicting the key features of the diurnal cycle of low cloud (Figs. 10c,d). The higher amplitude over land as compared to that over ocean was well captured by these products. Over the western Pacific Ocean, the phase of the low clouds was remarkably well simulated by the unified scheme and the superensemble. The pattern correlations for the unified scheme and the superensemble during day 5 of forecasts were 0.81 and 0.94, respectively. This shows that the unified cloud scheme and the superensemble were able to forecast the diurnal variation of high and low clouds realistically both over the equatorial land and oceanic regions up to 5 days in advance.

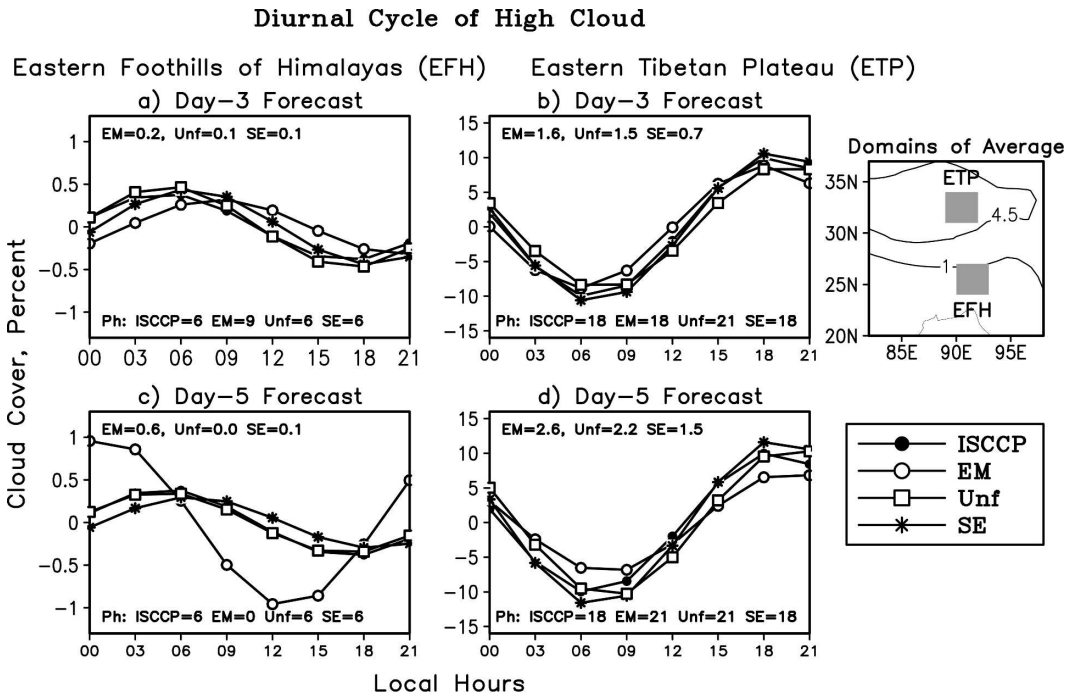

FIG. 11. Diurnal cycle of high cloud cover over the EFH (24°–27°N, 90°–93°E) and ETP (31°–34°N, 89°–92°E) from ISCCP and days 3 and 5 of forecasts from EM, Unified, and SE during 22–31 Mar 2000. RMS errors (in percent) of the total diurnal cycle for EM, Unified, and SE are indicated at the top of each panel. Also indicated is the phase of the diurnal cycle at the bottom of each panel. The regions of average are shown as shaded rectangles at the rhs with 1.0- and 4.5-km orography contours.

d. Performance over smaller domains

1) DIURNAL CYCLE OVER EASTERN HIMALAYAN REGION

One of the most significant contrasts in the phase of the diurnal cycle of high cloud and the associated precipitation within a small spatial scale are found over ETP and at EFH near the Indian state of Assam. Over the ETP the phase of the diurnal cycle of high cloud is in the afternoon hours, and over the EFH the phase is in the early morning hours. Here we shall illustrate the performances of the member models, the unified cloud scheme, and the superensemble in predicting this contrast of the phase of the diurnal cycle of high cloud cover.

Two 3° × 3° boxes representing these two regions are shown on the rhs of Fig. 11. Also shown in that panel are the 1.0- and 4.5-km orography contours. Over this region, within a distance of about 400 km from north to south, the terrain elevation increases from 1.0 to 4.5 km, and the phase of high cloud shifts from morning to afternoon hours. The ISCCP data showed the peak of the diurnal cycle at 0600 LT over the EFH (Figs. 11a,c), and at 1800 LT over the ETP (Figs. 11b,d). For day 3 of forecasts over the EFH (Fig. 11a), the ensemble mean of the four cloud schemes showed comparable amplitude of the diurnal cycle but the phase was 3 h later than the ISCCP satellite–based estimates. The diurnal cycle of the unified scheme and the superensemble followed closely those of the ISCCP satellite–based estimates. Over the ETP (Fig. 10b), all of the forecast products showed close correspondence to the ISCCP datasets.

The errors from the ensemble mean were particularly large over EFH during day 5 (Fig. 11c). Over this region, the amplitude from the ensemble mean of the cloud schemes was almost twice that of and the phase was 6 h earlier than the ISCCP datasets. The diurnal cycle from the unified scheme and the superensemble followed closely that of the ISCCP datasets. Over ETP (Fig. 11d), the amplitude of the diurnal cycle from the ensemble mean was of the same order as that of the ISCCP and the error in phase was 3 h. Again, the unified cloud scheme and the superensemble showed very high performance in predicting this afternoon maximum of high clouds over the ETP. This result shows that both the unified cloud scheme and the superensemble were able to predict the contrast in phase and amplitude of the diurnal cycle of high clouds over EFH and ETP during days 3 and 5 of forecasts. On the other hand, the accuracy of the ensemble mean fore-

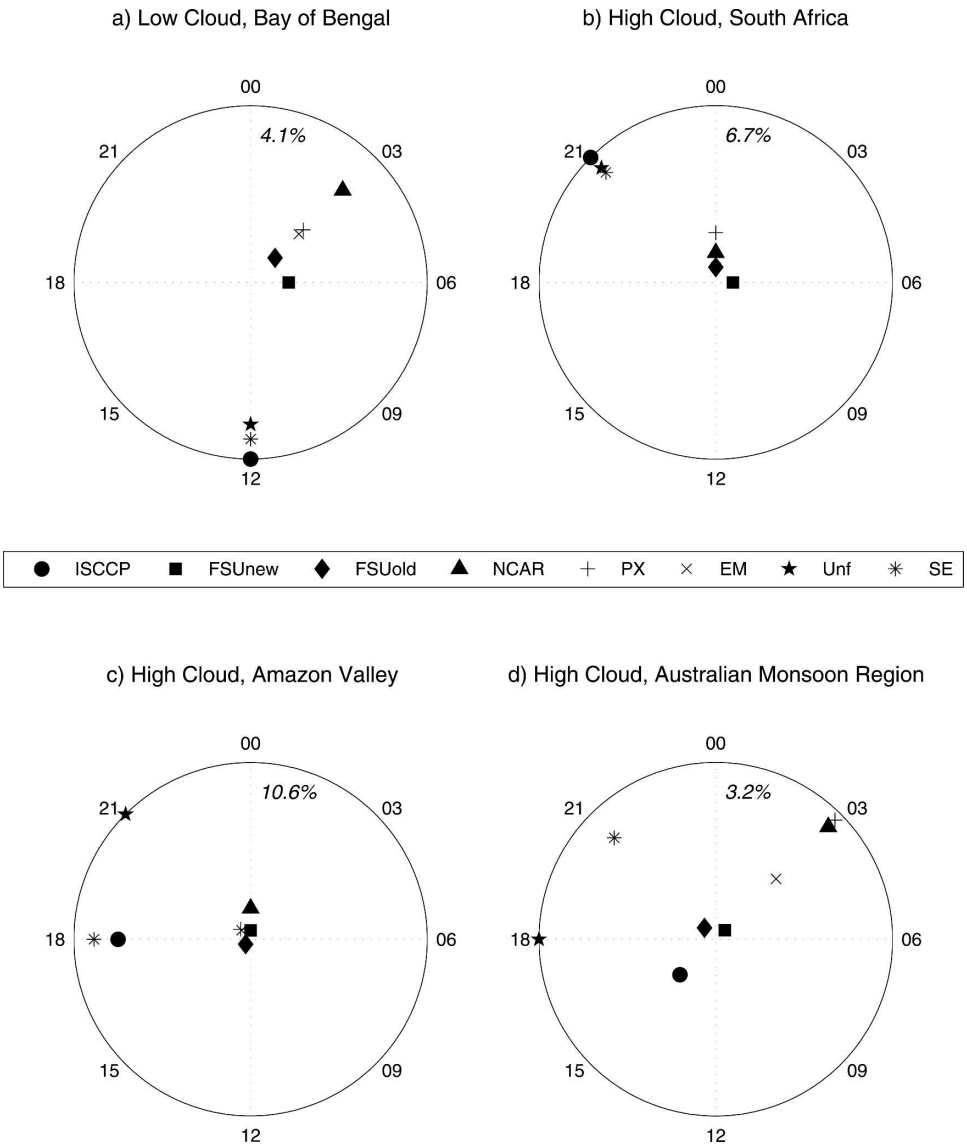

FIG. 12. Sundial representation of the phase and amplitude of the diurnal cycle of low and high clouds over (a) the Bay of Bengal (0°–20°N, 80°–100°E), (b) South Africa (35°–5°S, 10°–40°E), (c) Amazon valley (15°–5°S, 60°–50°W), and (d) Australian monsoon region (20°S–0°, 120°–140°E) from ISCCP and day-5 forecast of the four member models, their ensemble mean, the unified cloud scheme, and the SE during 22–31 Mar 2000. The representative amplitude of the radius of each dial is indicated by the number at the top (near 0 h) in percent.

casts decreased from day 3 to day 5 over both of these domains.

2) DIURNAL CYCLE OVER A FEW OTHER IMPORTANT AREAS AROUND THE WORLD

The diurnal cycle of low clouds over the Bay of Bengal and surrounding region (0°–20°N, 80°–100°E), South Africa (35°–5°S, 10°–40°E), the Amazon valley (35°–5°S, 50°–60°W), and the Australian monsoon region (20°S–0°, 120°–140°E) is shown in Fig. 12 from ISCCP data and for day 5 of forecasts from the member cloud schemes, their ensemble mean, the unified cloud scheme, and the superensemble using a sundial representation (Wallace 1975). In this representation, the radius of the dial is representative of the normalized amplitude of the diurnal cycle and the angle is representative of the phase. A phase of 0000 LT (local midnight) is represented by a point at the north, and a phase of 0600 LT (local morning) is represented by a point at the east, and so on. In this figure the normalization factor

for the amplitude (the radius of the dial) is indicated at the top of each dial.

Over the Bay of Bengal and surrounding land areas (Fig. 12a), low clouds estimated from the ISCCP satellite observations showed a peak at 1200 LT. The amplitude of this diurnal cycle was 4.1%. None of the member models were able to capture this phase during the noon hour. Moreover, amplitude was also underestimated by most of the member models. On the other hand, both the unified scheme and the superensemble could correctly simulate the phase and amplitude of the diurnal cycle.

Over South Africa (Fig. 12b), high clouds showed a diurnal peak at 2100 LT as obtained from the ISCCP satellite estimates. No models were able to capture this phase during day 5 of forecasts. Moreover, the amplitude of the diurnal cycle was much less in the member models as compared to the ISCCP estimates. It was possible to correct the phase and amplitude of the high clouds over this region with the unified cloud scheme and the superensemble.

The Amazon valley (Fig. 12c) is one of the heaviest rainfall regions on the earth. The highest seasonal rainfall over this region occurs during January–March [above 46% of the total annual rainfall during these 3 months and above 14% during March alone; based on 1979–2004 climatology from Xie and Arkin (1997)]. It is of interest to study the diurnal cycle of high clouds over this region from satellite observations and from forecasts. It was found from the ISCCP datasets that high clouds had a peak at 1800 LT with an amplitude of about 8% over this region. The performance of the member models was quite poor during day 5 of forecasts. The amplitude of the diurnal cycle from all the member models was below 2% and the phase was at 1500–2100 LT. The ensemble mean also showed similar phase and amplitude errors. The unified cloud scheme had a phase error of 3 h but its amplitude was closer to that of the ISCCP data. Phase and amplitude of the superensemble forecasts were very close to the ISCCP satellite–based estimates.

High clouds over the Australian monsoon region (Fig. 12d) from the ISCCP estimation showed a diurnal peak at 1500 LT. None of the member models and their ensemble mean were able to predict this phase correctly. In fact, the member models showed their peak at 0300 LT, a 180° shift in phase. The unified cloud scheme showed a peak at 1800 LT and the superensemble showed a peak at 2100 LT for high clouds over this region. Although the phase error for these products was 3 and 6 h, it was possible to forecast a better phase compared to the member models.

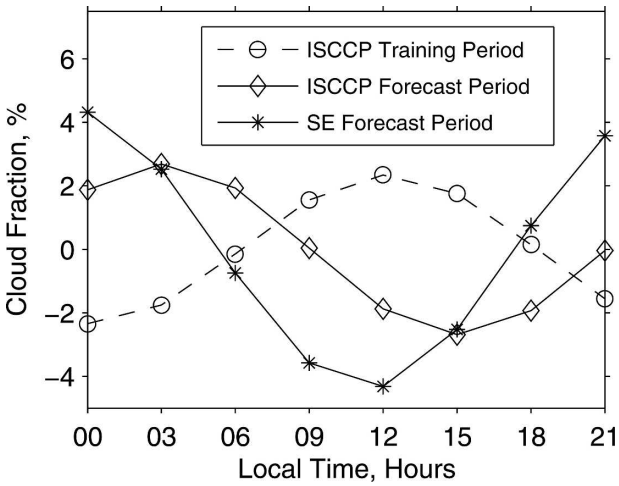

FIG. 13. Diurnal cycle of high clouds over the equatorial Indian Ocean (5°S–5°N, 90°–100°E) during the SE training period (1 Jan–21 Mar) from ISCCP-based observations and SE forecast period (22 Mar–31 Mar) from ISCCP-based observations and SE forecasts. This figure shows that the phase information contained in the observed data during the training period does not affect the phase of the SE forecast, which is closer to the observed phase during the forecast period.

e. Training climatology and its impact on forecast

Figure 13 shows the diurnal cycle of high clouds over the equatorial Indian Ocean (5°S–5°N, 90°–100°E) from ISCCP satellite estimates and superensemble forecasts. The phase of the diurnal cycle of high clouds in the ISCCP observations changes from the noon hours (1200 LT) in the training period to early morning hours (0300 LT) in the forecast period. The superensemble, although it was trained by the ISCCP estimates for the training period, was able to capture this early morning phase during the forecast period quite well. This clearly shows that the training period climatology of the observed data does not affect the forecast characteristics of the superensemble. The training period is used for a collective bias removal of the member models and to calculate the weights to use in the forecast phase. When the model biases remain similar during the training and forecasts periods, the superensemble consensus forecast, due to its collective bias removal, has a higher accuracy compared to the member models.

7. Improvements in radiation budget

In this section we ask the question of how well these models handle the TOA longwave and shortwave radiation fluxes in a monthly mean time scale. This longer time scale was chosen as opposed to 3-hourly averages (which were used otherwise in this study) to examine if

TABLE 3. Spatial correlations (SC) and root mean square error (RMSE; W m^{-2}) of OLR from EM and Unified cloud scheme over Tropics and subtropics (40°S–40°N, 0°–360°E) during day 3 and day 5 of forecasts averaged over March 2000.

	Day 3		Day 5	
	SC	RMSE	SC	RMSE
EM	0.67	20.6	0.58	22.1
Unified	0.85	15.7	0.83	18.3

the unified scheme has a positive impact on radiative parameters on the climate time scale as well. Radiative fluxes estimated from CERES PFM instruments aboard TRMM satellites are considered the benchmark for computing the performance parameters for forecast accuracy. The fluxes from CERES were calculated from hourly monthly mean values by averaging over 24 h of the day. Construction of a superensemble was not possible here because the forecasting of monthly mean radiative parameters from the superensemble would require several years of model simulation. Monthly mean training data for only two months (January and February 2000) were not sufficient to obtain a stabilized set of weights for forecasts during March 2000.

Table 3 shows the spatial correlations with observations (CERES satellite–based estimates) and RMS errors of OLR from the ensemble mean of the member models and the unified cloud scheme over the Tropics and subtropics (40°S–40°N, 0°–360°E) for the month of March 2000. During day 3 (day 5) of forecasts, it was possible to increase the spatial correlation by 0.18 (0.27) and decrease the RMS error by 4.9 (3.8) W m^{-2} as compared to the ensemble mean with the use of the unified cloud scheme. This order of improvement was consistent with the results obtained by Bergman and Salby (1997), who showed that there can be errors on the order of 5 W m^{-2} in the estimation of longwave flux at the TOA if the diurnal cycle was not taken into account. It was noticed that this improvement in the spatial correlations and RMS errors were due to the better estimation of OLR by the unified scheme compared to the ensemble mean, especially over the highly cloud-covered (and associated low OLR) areas in this summer month of the Southern Hemisphere (namely, the Australian monsoon region, the Amazon valley, and South Africa).

Figure 14 shows 3-hourly variation of monthly mean OLR over the Australian monsoon region (20°S–0°, 120°–140°E) and Amazon valley (15°–5°S, 60°–50°W) during March 2000 from CERES data and day-5 forecasts of the four cloud schemes, their ensemble mean, and the unified cloud scheme. All of the member cloud schemes and their ensemble means showed higher values of OLR compared to the observation (CERES). Errors varied from 20–50 W m^{-2} over the Australian monsoon region to about 80 W m^{-2} over the Amazon valley for the member cloud schemes. The errors were reduced to within 5 W m^{-2} with the use of the unified cloud scheme. The peak of the diurnal cycle of OLR (at 0900–1200 LT) over both these regions and the larger amplitude of variation over land (Amazon valley) as compared to that over ocean (Australian monsoon region) were also well predicted by the unified scheme. Those features were poorly handled by the member models. In summary, these results show that forecasting of the upward longwave flux at the TOA was possible

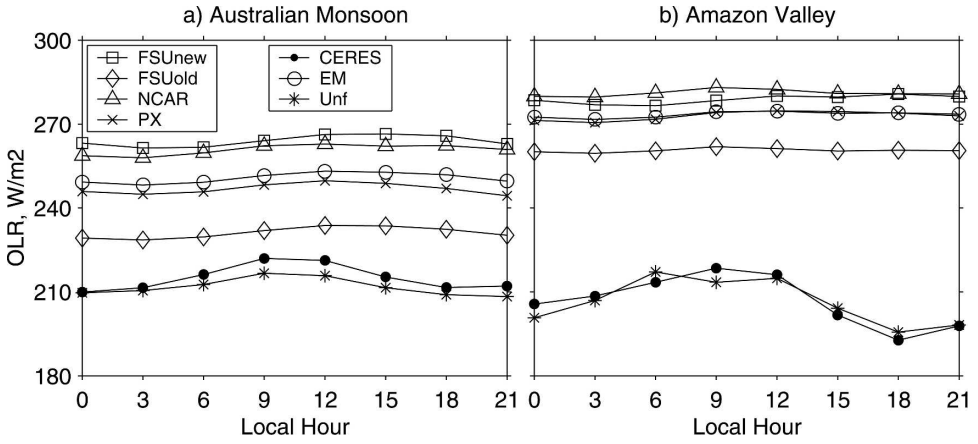

FIG. 14. Comparison of 3-hourly variation of monthly mean outgoing longwave radiation (W m^{-2}) at the TOA during March 2000 from observation (CERES), four cloud schemes, their ensemble mean, and the unified cloud scheme developed in this study over the (a) Australian monsoon domain (20°S–equator, 120°–140°E) and (b) Amazon valley (15°–5°S, 60°–50°W).

with a higher accuracy using the unified cloud scheme when compared to individual member models that carry a single cloud scheme each.

Similar results were obtained for reflected shortwave radiation at the TOA (not shown). The RMS error of the outgoing shortwave flux at the TOA was reduced by 5.8 W m^{-2} during day 3 and 9.4 W m^{-2} during day 5 of forecasts with the use of the unified cloud scheme as compared to the ensemble mean for the month of March 2000. The unified cloud scheme also reduced the bias of the shortwave radiation by 22.6 and 24.7 W m^{-2} during days 3 and 5 of forecasts, respectively. These results show that the radiation budget at the TOA was greatly improved when the unified cloud scheme was used in a single model as compared to the multimodel ensemble.

8. Conclusions

The major finding of this study was that it was possible to substantially reduce the error of the current cloud parameterization schemes for predicting the diurnal cycle with a multimodel superensemble approach out to 5 days in advance. The merit of this approach lied in assigning geographically varying weights to each of the member models. The weights were determined from the past performance of each of the models. This enabled the removal of the collective bias of the models, resulting in improved forecasts of the diurnal cycle.

Observation-based data showed that a peak of the diurnal cycle of high clouds follows that of the low clouds by about 6 h both over tropical land and oceans. In general, a noon–afternoon maximum was noticed over land and a early morning–morning maximum over oceans. However, there were important exceptions. For example, over the tropical Indian Ocean, the peak of the diurnal cycle of low clouds occurs during noon hours, about 6 h later compared to that over the western Pacific Ocean.

It was found that each of the four diagnostic cloud parameterization schemes used in this paper carried large forecast errors for the phase and amplitude of the diurnal cycle for low and high clouds. Particularly large phase errors were noted over the oceans. Most of the individual cloud schemes showed a very weak geographical variation of the diurnal mode over most of the regions over the Tropics. It is possible that a prognostic cloud scheme (Sundqvist 1978; Sundqvist et al. 1989), if used as a member of the ensemble, will perform better compared to the diagnostic cloud schemes used in this study. However, the accuracies of the superensemble and the unified cloud scheme in forecasting the diurnal cycle of clouds will still most likely exceed those of the prognostic scheme, since any bias associated with the prognostic scheme will be removed by the superensemble methodology.

Encouraged by a superior performance of the superensemble, this study developed a new unified cloud parameterization scheme for global climate models that utilized a weighted mean of cloud schemes derived from the multimodel superensemble. Four cloud schemes were run in parallel inside a single GCM and their forecasts of cloud fraction were combined, based on their past performance, to derive a unified cloud scheme forecast. This new cloud parameterization scheme improved the 1–5 days of forecast of the diurnal cycle of cloud cover compared to the other individual cloud models.

This unified scheme was an integral part of a model and thus had the potential to carry improved forecasts for other parameters. It was found that the prediction of monthly mean outgoing longwave radiation and its diurnal cycle over the Tropics and midlatitudes was greatly improved when the unified cloud scheme was implemented within a GCM. This shows the possibility that the unified cloud scheme can have greater impact on the climate time scale. Such a unified model needs to be tested for seasonal prediction.

Given that it is now possible to predict the phase and amplitude of the diurnal mode reasonably correctly out to 5 days, we ask how we can exploit this further. It is important to improve a single model from this postprocessing of the superensemble. The unified modeling is one avenue to be explored in future modeling studies. Separate unified schemes for different physical parameterizations such as cloud, planetary boundary layer, and cumulus convection can be deployed in a single model to improve its overall performance.

Acknowledgments. We gratefully acknowledge ECMWF for providing the initial conditions for model simulations. ISCCP cloud data and CERES radiative fluxes were taken from NASA Langley Research Center's ASDC Web site. This study is supported by NSF Grant ATM-0491618, NASA Grants NAGS-13563 and NNG05GH81G, and NOAA Grant NA16GP1365.

REFERENCES

Bergman, J. W., 1997: A numerical investigation of cloud diurnal variations. *J. Climate,* **10,** 2330–2350.

——, and M. L. Salby, 1996: Diurnal variations of cloud cover and their relationship to climatological conditions. *J. Climate,* **9,** 2802–2820.

——, and ——, 1997: The role of cloud diurnal variations in the time-mean energy budget. *J. Climate,* **10,** 1114–1124.

Betts, A. K., and C. Jakob, 2002a: Evaluation of the diurnal cycle of precipitation, surface thermodynamics, and surface fluxes

in the ECMWF model using LBA data. *J. Geophys. Res.,* **107,** 8045, doi:10.1029/2001JD000427.

——, and ——, 2002b: Inferences of predictability associated with warm season precipitation episodes. *J. Atmos. Sci.,* **59,** 2033–2056.

Chakraborty, A., and T. N. Krishnamurti, 2006: Improved seasonal climate forecasts of the south Asian summer monsoon using a suite of 13 coupled ocean–atmosphere models. *Mon. Wea. Rev.,* **134,** 1697–1721.

Chen, S. S., and R. A. Houze Jr., 1997: Diurnal variation and life-cycle of deep convective systems over the tropical pacific warm pool. *Quart. J. Roy. Meteor. Soc.,* **123,** 357–388.

Dai, A., 2001: Global precipitation and thunderstorm frequencies. Part II: Diurnal variations. *J. Climate,* **14,** 1112–1128.

——, 2006: Precipitation characteristics in eighteen coupled climate models. *J. Climate,* **19,** 4605–4630.

——, and C. Deser, 1999: Diurnal and semidiurnal variations in global surface wind and divergence fields. *J. Geophys. Res.,* **104,** 31 109–31 126.

——, and K. E. Trenberth, 2004: The diurnal cycle and its depiction in the Community Climate System Model. *J. Climate,* **17,** 930–951.

——, F. Giorgi, and K. E. Trenberth, 1999: Observed and model-simulated precipitation diurnal cycle over the contiguous United States. *J. Geophys. Res.,* **104,** 6377–6402.

——, T. R. Karl, B. Sun, and K. E. Trenberth, 2006: Recent trends in cloudiness over the United States. *Bull. Amer. Meteor. Soc.,* **87,** 597–606.

Hamill, T. M., J. S. Whitaker, and X. Wei, 2004: Ensemble reforecasting: Improving medium-range forecast skill using retrospective forecasts. *Mon. Wea. Rev.,* **132,** 1434–1447.

Janowiak, J. E., V. E. Kousky, and R. J. Joyce, 2005: Diurnal cycle of precipitation determined from the cmorph high spatial and temporal resolution global precipitation analysis. *J. Geophys. Res.,* **110,** D23105, doi:10.1029/2005JD006156.

Krishnamurti, T. N., and J. Sanjay, 2003: A new approach to the cumulus parameterization issue. *Tellus,* **55,** 275–300.

——, C. M. Kishtawal, T. E. LaRow, D. R. Bachiochi, Z. Zhang, C. E. Williford, S. Gadgil, and S. Surendran, 1999: Improved weather and seasonal climate forecasts from multimodel superensemble. *Science,* **285,** 1548–1550.

——, ——, D. W. Shin, and C. E. Williford, 2000: Multimodel superensemble forecasts for weather and seasonal climate. *J. Climate,* **13,** 4196–4216.

——, and Coauthors, 2003: Improved skill for the anomaly correlation of geopotential heights at 500 hPa. *Mon. Wea. Rev.,* **131,** 1082–1102.

——, A. Chakraborty, R. Krishnamurti, W. K. Dewar, and C. A. Clayson, 2006a: Seasonal prediction of sea surface temperature anomalies using a suite of 13 coupled atmosphere–ocean models. *J. Climate,* **19,** 6069–6088.

——, A. K. Mitra, W.-T. Yun, and T. S. V. V. Kumar, 2006b: Seasonal climate forecasts of the Asian monsoon using multiple coupled models. *Tellus,* **58A,** 487–507.

——, C. Gnanaseelan, and A. Chakraborty, 2007: Prediction of the diurnal cycle using a multimodel superensemble. Part I: Precipitation. *Mon. Wea. Rev.,* **135,** 3613–3632.

Murakami, M., 1983: Analysis of the deep convective activity over the tropical western Pacific. *J. Meteor. Soc. Japan,* **61,** 60–77.

Pleim, J. E., and A. Xiu, 1995: Development and testing of a surface flux and planetary boundary layer model for application in mesoscale models. *J. Appl. Meteor.,* **34,** 16–32.

Randall, D. A., Harshvardhan, and D. A. Dazlich, 1991: Diurnal variability of the hydrologic cycle in a general circulation model. *J. Atmos. Sci.,* **48,** 40–62.

Reynolds, R. W., and T. M. Smith, 1994: Improved global sea surface temperature analysis using optimum interpolation. *J. Climate,* **7,** 929–948.

Rossow, W. B., and R. A. Schiffer, 1999: Advances in understanding clouds from ISCCP. *Bull. Amer. Meteor. Soc.,* **80,** 2261–2287.

——, A. W. Walker, and L. C. Garder, 1993: Comparison of ISCCP and other cloud amounts. *J. Climate,* **6,** 2394–2418.

Rozendaal, M. A., C. B. Leovy, and S. A. Klein, 1995: An observational study of diurnal variations of marine stratiform cloud. *J. Climate,* **8,** 1795–1809.

Shin, K.-S., G. R. North, Y.-S. Ahn, and P. A. Arkin, 1990: Time scales and variability of area-averaged tropical oceanic rainfall. *Mon. Wea. Rev.,* **118,** 1507–1516.

Slingo, J. M., 1987: The development and verification of a cloud prediction scheme for the ECMWF model. *Quart. J. Roy. Meteor. Soc.,* **113,** 899–927.

——, P. Inness, R. Neale, S. Woolnough, and G.-Y. Yang, 2003: Scale interactions on diurnal to seasonal timescales and their relevance to model systematic errors. *Ann. Geophys.,* **46,** 139–155.

Stefanova, L., and T. N. Krishnamurti, 2002: Interpretation of seasonal climate forecast using Brier skill score, FSU superensemble, and the AMIP-I data set. *J. Climate,* **15,** 537–544.

Sundqvist, H., 1978: A parameterization scheme for non-convective condensation including prediction of cloud water content. *Quart. J. Roy. Meteor. Soc.,* **104,** 677–690.

——, E. Berge, and J. E. Kristjnsson, 1989: Condensation and cloud studies with a mesoscale numerical weather prediction model. *Mon. Wea. Rev.,* **117,** 1641–1657.

Tian, B., B. J. Soden, and X. Wu, 2004: Diurnal cycle of convection, clouds, and water vapor in the tropical upper troposphere: Satellites versus a general circulation model. *J. Geophys. Res.,* **109,** D10101, doi:10.1029/2003JD004117.

Trenberth, K. E., A. Dai, R. M. Rasmussen, and D. B. Parsons, 2003: The changing character of precipitation. *Bull. Amer. Meteor. Soc.,* **84,** 1205–1217.

Wallace, J. M., 1975: Diurnal variations in precipitation and thunderstorm frequency over the conterminous United States. *Mon. Wea. Rev.,* **103,** 403–419.

Williford, C. E., T. N. Krishnamurti, R. C. Torres, S. Cocke, Z. Christidis, and T. S. V. Kumar, 2003: Real-time multimodel superensemble forecasts of Atlantic tropical systems of 1999. *Mon. Wea. Rev.,* **131,** 1878–1894.

Xie, P., and P. A. Arkin, 1997: A 17-year monthly analysis based on gauge observations, satellite estimates, and numerical model outputs. *Bull. Amer. Meteor. Soc.,* **78,** 2539–2558.

Yang, G.-Y., and J. Slingo, 2001: The diurnal cycle in the Tropics. *Mon. Wea. Rev.,* **129,** 784–801.

Yang, S., and E. A. Smith, 2006: Mechanisms for diurnal variability of global tropical rainfall observed from TRMM. *J. Climate,* **19,** 5190–5226.

Yun, W.-T., L. Stefanova, and T. N. Krishnamurti, 2003: Improvement of the multimodel superensemble technique for seasonal forecasts. *J. Climate,* **16,** 3834–3840.

Yussouf, N., and D. J. Stensrud, 2006: Prediction of near-surface variables at independent locations from a bias-corrected ensemble forecasting system. *Mon. Wea. Rev.,* **134,** 3415–3424.